

Temperature dependence of the dielectric function in the spectral range (0.5–8.5) eV of an In_2O_3 thin film

R. Schmidt-Grund, H. Krauß, C. Kranert, M. Bonholzer, and M. Grundmann

Citation: *Appl. Phys. Lett.* **105**, 111906 (2014); doi: 10.1063/1.4896321

View online: <https://doi.org/10.1063/1.4896321>

View Table of Contents: <http://aip.scitation.org/toc/apl/105/11>

Published by the [American Institute of Physics](http://www.aip.org)

Articles you may be interested in

[Dielectric function in the NIR-VUV spectral range of \$\(\text{In}_x\text{Ga}_{1-x}\)_2\text{O}_3\$ thin films](#)

Journal of Applied Physics **116**, 053510 (2014); 10.1063/1.4891521

[Dielectric tensor of monoclinic \$\text{Ga}_2\text{O}_3\$ single crystals in the spectral range 0.5–8.5 eV](#)

APL Materials **3**, 106106 (2015); 10.1063/1.4934705

[Optical properties of gallium oxide thin films](#)

Applied Physics Letters **81**, 250 (2002); 10.1063/1.1491613

[Dielectric function in the spectral range \(0.5–8.5\)eV of an \$\(\text{Al}_x\text{Ga}_{1-x}\)_2\text{O}_3\$ thin film with continuous composition spread](#)

Journal of Applied Physics **117**, 165307 (2015); 10.1063/1.4919088

[Temperature dependent dielectric function in the near-infrared to vacuum-ultraviolet ultraviolet spectral range of alumina and yttria stabilized zirconia thin films](#)

Journal of Applied Physics **114**, 223509 (2013); 10.1063/1.4844515

[High electron mobility \$\text{In}_2\text{O}_3\(001\)\$ and \(111\) thin films with nondegenerate electron concentration](#)

Applied Physics Letters **97**, 072103 (2010); 10.1063/1.3480416

AIP | Conference Proceedings

Get **30% off** all
print proceedings!

Enter Promotion Code **PDF30** at checkout



Temperature dependence of the dielectric function in the spectral range (0.5–8.5) eV of an In₂O₃ thin film

R. Schmidt-Grund,^{a)} H. Krauß, C. Kranert, M. Bonholzer, and M. Grundmann
 Institut für Experimentelle Physik II, Universität Leipzig, Linnéstr. 5, 04103 Leipzig, Germany

(Received 11 July 2014; accepted 9 September 2014; published online 19 September 2014)

We present the dielectric function of a bcc-In₂O₃ thin film in the wide spectral range from near-infrared to vacuum-ultraviolet and for temperatures 10 K–300 K, determined by spectroscopic ellipsometry. From the temperature dependence of electronic transition energies, we derive electron-phonon coupling properties and found hints that the direct parabolic band-band transitions involve In-*d* states. Further we discuss possible excitonic contributions to the dielectric function. © 2014 AIP Publishing LLC. [<http://dx.doi.org/10.1063/1.4896321>]

In the last years, crystalline In₂O₃ has come in the focus of research caused by its properties promising for transparent electronics as, e.g., high electron mobilities¹ and its large band gap. Besides applications such as transparent conductive layers and channels in transparent field effect transistors, recent progress in Schottky contacts on In₂O₃ makes it also interesting for metal-semiconductor field effect transistors.² For these applications, high-quality thin films rather than bulk material are mandatory whose electronic band structure properties and the dielectric function as well as the absorption coefficient and refractive index have to be known.

The electronic and optical properties in the near-infrared to vacuum-ultraviolet spectral range of In₂O₃ have been thoroughly studied theoretically^{3–8} but less comprehensively in experiment^{8–13} as discussed in Ref. 17. Summarizing, detailed knowledge of properties of the dielectric function is missing so far, especially as a function of temperature. Irmischer *et al.*¹³ reported on the temperature dependence of the fundamental band gap energy and the absorption coefficient in its vicinity between 9 K and 1273 K determined from high-quality bulk single crystals. They could clarify the question of dipole allowed indirect or dipole forbidden direct band-band transitions characterizing the onset of absorption: the spectral lineshape of the absorption coefficient α suggests an indirect transition energetically closely followed by the dipole forbidden direct transition to be the nature of the optical band gap of bcc-In₂O₃. The indirect transition is mediated by optical phonons with an energy of ≈ 45 meV. From the strong temperature dependence of the band gap energy, they derived mean energies of phonons involved in the electron-phonon coupling in the range between ≈ 18 meV and 54 meV.¹³ Considering the large number of phonon modes of bcc-In₂O₃ distributed in a large energy range,¹⁴ one can expect much more complicated properties of electron-phonon interaction by individual oscillators accruing in small temperature steps up to very elevated temperatures. The observed exceptionally strong band gap shrinkage which was ascribed to a large electron-phonon coupling strength¹³ may be rather caused in that large number of phonon branches.

In this letter, we present the dielectric function (DF) of a bcc-In₂O₃ thin film for temperatures 10–300 K and energies (0.5–8.5) eV and discuss the temperature dependence of electronic band-band transitions.

The 690 nm thick In₂O₃ film was grown by means of pulsed laser deposition on a (111)-oriented YSZ substrate (YSZ: yttria stabilized zirconia) at an oxygen pressure of 0.002 mbars and a substrate temperature of 700 °C. Atomic force microscopy reveals a smooth surface with small grains and a roughness of $R_{\text{rms}} \approx 1$ nm. X-ray diffraction reveals a high quality (111) oriented bcc-In₂O₃ film (see Ref. 15). This is also reflected by the phonon mode properties which have been investigated by means of Raman spectroscopy and which are similar to that discussed in Ref. 14. The DF was determined by means of spectroscopic ellipsometry with subsequent model analysis using numeric (Kramers-Kronig consistent mathematical inversion using B-spline functions) and parameterized model dielectric functions (MDF). Examples for the model approximation to the experimental data are shown in Fig. 1, which displays spectra of the pseudo dielectric function $\langle \tilde{\epsilon} \rangle = \langle \epsilon_1 \rangle + i \langle \epsilon_2 \rangle$.^{15,16} From the DF, we derived the refractive index and absorption coefficient and parameters of electronic transitions. More details on the ellipsometry model analysis and the used model dielectric functions

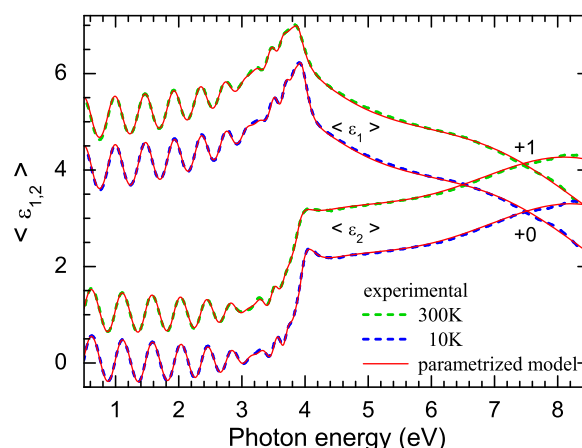


FIG. 1. Experimental (dashed lines) and parametrized model calculated (approach (II), solid lines) spectra of the pseudo dielectric functions $\langle \epsilon_{1,2} \rangle$ for 10 K and 300 K and for an angle of incidence $\phi = 70^\circ$. The spectra are shifted vertically against each other for clarity as indicated.

^{a)}Schmidt-Grund@physik.uni-leipzig.de

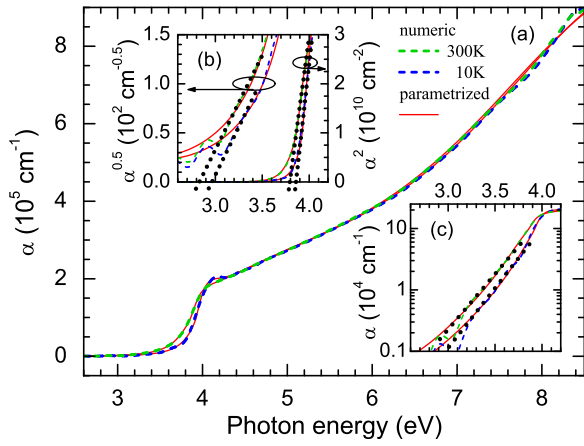


FIG. 2. (a) Absorption coefficient α for 10 K and 300 K. The inset (b) shows $\alpha^{0.5}$ and α^2 , the inset (c) α in a logarithmic scale in the near band gap spectral range. Dashed and solid lines are data calculated from the numeric and parameterized (approach (II)) MDF, respectively. The dotted lines in (b) and (c) represent linear extrapolation towards zero.

can be found in the supplemental material Ref. 15 and in Refs. 17 and 18.

The film is transparent in the spectral range below 2.5 eV and the optical response is described by the real part of the refractive index n using the Cauchy model¹⁶

$$n(\lambda, T) = (1.9982 + 3 \times 10^{-6} \text{K}^{-1} \cdot T + 7 \times 10^{-8} \text{K}^{-2} \cdot T^2) + (0.02825 \mu\text{m}^2 + 3 \times 10^{-6} \mu\text{m}^2 \text{K}^{-1} \cdot T) / \lambda^2,$$

with λ being the vacuum wavelength of light and T the temperature.

Spectra of the absorption coefficient α derived from the MDF are shown in Fig. 2 along with their logarithmic, quadratic, and square root depiction. As pointed out in Ref. 13, the onset of absorption for bcc-In₂O₃ should mainly be proportional to $\alpha^{0.5}$ spectrally closely followed by $\alpha \propto \alpha^{2/3}$ due to the indirect and dipole forbidden direct band gap. The line-shape of α obtained from the numeric DF do not clearly show such a behaviour, partially caused by data uncertainty due to effects introduced by the cryostat windows to very low values of α . But the inferior crystal quality of our thin film compared to bulk material will be the main reason. Our data show an exponential low-energy Urbach-like absorption tail probably due to disorder, by trend superimposed by an $\alpha^{0.5}$ -behaviour, followed at higher energies by a clear α^2 increase, typical for allowed direct transitions between parabolic bands. Linear extrapolation of $\alpha^{0.5}$ and α^2 to zero yield for the phonon emission indirect band edge type 2.96 eV (2.83 eV), similar to values from literature¹³ (note the larger uncertainty here of $\approx \pm 0.05$ eV), and for the parabolic direct band gap 3.86 eV (3.80 eV) for 10 K (300 K). The absorption edge is followed at higher energies by a peak-like structure, which is clearly present at 10 K and broadens respectively vanishes almost towards room temperature. Such properties could hint to excitonic effects, which already have been observed in photoluminescence and thermoreflectance experiments yielding a binding energy of the free exciton ground state of 40 meV, which is about 1.5 times the thermal energy at room temperature.^{19–21} But also band-band

transitions involving bands with disorder induced non-parabolicity could induce such a lineshape.²² At further high energies, the absorption increases without pronounced structures and α equals almost for all temperatures.

Based on the lineshape of α , we pursued two different approaches for the parameterized model DF, namely, considering (I) excitonic effects and (II) disorder induced non-parabolic bands (for more details see supplementary material in Ref. 15). In each case, we used the simplest model with as little as possible degrees of freedom to avoid parameter correlation. The DF near the absorption edge is described by (I) a Tanguy lineshape function,^{23,24} which considers the sum of discrete and continuum exciton states and a M0 critical point function for parabolic direct band-band transitions (“CPM0” with energy E_{CPM0}).^{25,26} The energy of the exciton continuum edge and E_{CPM0} have been set to be equal. In approach (II), a Tauc-Lorentz oscillator for the non-parabolic contributions and the low energy absorption by the indirect and forbidden direct transitions (“TcLo” with central energy of the Lorentzian contribution E_n and the Tauc-gap E_g),²² combined with a CPM0 function for the contributions of transitions involving parabolic bands have been chosen. Here, E_n and E_{CPM0} have been allowed to be independent of each other. In both cases, a Gaussian oscillator follows at higher energies to account for transitions which are spread within the Brillouin zone (“Gaussian,” E_{Gaussian}). A pole function (“Pol”) is used in order to account for contributions to ε_1 of electronic transitions at energies higher than the spectral range investigated.

Spectra of the real and imaginary parts of the DF $\tilde{\varepsilon} = \varepsilon_1 + i\varepsilon_2$ are shown in Fig. 3. The main panels show the numeric DF for $T=10$ K and the parameterized DF after approach (II) for all temperatures. Also their individual contributions are included in Fig. 3(b) exemplarily for $T=10$ K. The inset in Fig. 3(b) shows, exemplarily for $T=10$ K, a comparison between the MDF of approaches (I) and (II) in an enlarged section around the peak-like structure along with the individual contributions to approach (I). Clear differences between both are observable. While approach (II) yields an almost perfect match to the numeric DF (Fig. 3(b), main panel), the DF of approach (I) differs considerably around the peak-like structure (Fig. 3(b), inset) and also at the onset of absorption at low energies as well as at higher energies. This differences can be caused by sample non-ideality suggesting a combination of approaches (I) and (II). But by doing so, due to the large spectral broadening of the features even at low temperature, the parameter correlation becomes so large that no reliable parameters can be obtained. But already from approach (I), no information on the exciton properties can be obtained. Thus, at this point it cannot be judged unambiguously if the peak-like structure arises from excitonic effects or is purely caused by disorder effects. In the following, we will exclusively discuss results obtained by approach (II). The onset of absorption after (II) is dominated by the Tauc-Lorentz lineshape followed by a pronounced CPM0-type contribution. With increasing temperature, the peak caused by the Lorentzian part of the TcLo oscillator weakens and the broad shoulder at higher energies due to the CPM0 becomes more pronounced. Also, the expected red-shift of the absorption features and an increasing broadening of the onset of absorption are observable.

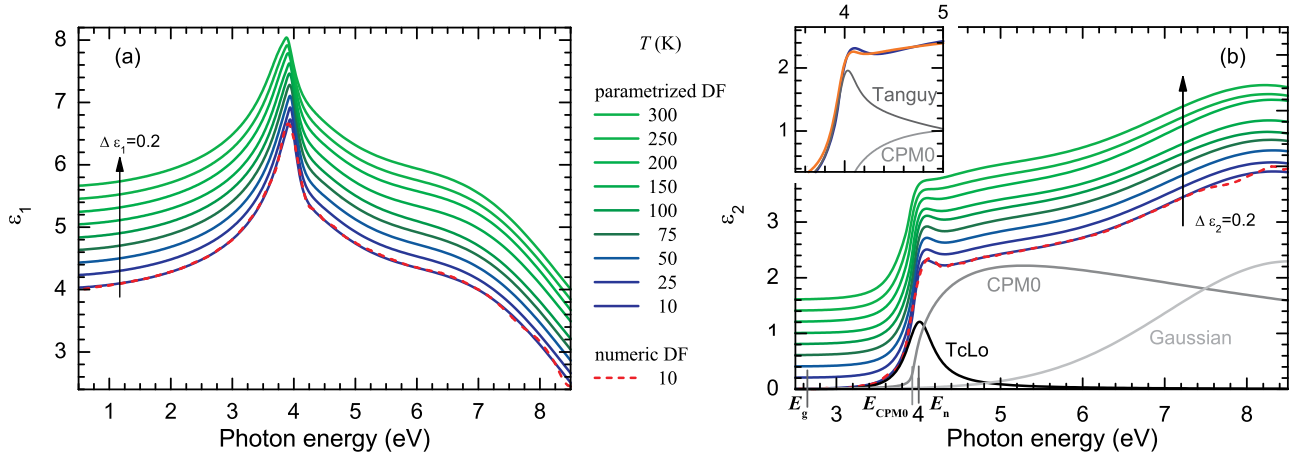


FIG. 3. Spectra of the (a) real (ϵ_1) and (b) imaginary parts (ϵ_2) of the DF for all temperatures studied. Solid and dashed lines represent the parameterized (approach (II)) and numeric DF, respectively. The spectra are shifted vertically against each other for clarity. The inset shows in an enlarged spectral range ϵ_2 for 10 K after approach (I) (orange line) and (II) (blue line). The individual contributions to both MDF for $T = 10$ K are shown in grey lines.

The temperature evolution of the energy parameters of the MDF contributions (approach (II)) is shown in Fig. 4. The redshift of the transition energies with increasing temperature due to electron-phonon interaction is reflected. It is noted that for the TcLo model $E_g(T)$ is somewhat noisy but an almost constant difference $E_n - E_g \approx 1.37 \pm 0.1$ eV is found. Thus, E_g is close to the energy of the indirect band gap,¹³ but at ≈ 200 meV lower energies reflecting its character as a measure for the Urbach absorption tail.²² E_n , E_g , and also E_{Gaussian} show a redshift between 10 K and 300 K of ≈ 100 meV. Surprisingly, E_{CPM0} shifts only by half that amount. $E_n(T)$ and $E_{\text{CPM0}}(T)$ have been approximated by the Bose-Einstein model for electron-phonon interaction^{15,18,27} (Fig. 4) yielding

(i) 0 K oscillator energies:

$$E_n(0 \text{ K}) = 3.998 (\pm 0.002) \text{ eV}$$

$$E_{\text{CPM0}}(0 \text{ K}) = 3.932 (\pm 0.002) \text{ eV}.$$

(ii) Mean phonon-branch energies:

$$E_{\text{BE-n}} = 26 (\pm 5) \text{ meV}$$

$$E_{\text{BE-CPM0}} = 20 (\pm 5) \text{ meV}.$$

(iii) Electron-phonon coupling strength parameter:

$$\alpha_{\text{BE-n}} = 0.53 (\pm 0.06) \text{ meV/K}$$

$$\alpha_{\text{BE-CPM0}} = 0.27 (\pm 0.04) \text{ meV/K}.$$

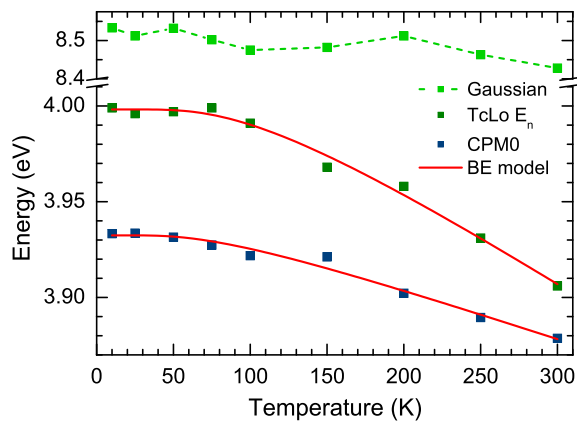


FIG. 4. Energy parameters of the MDF contributions (approach (II)) to the dielectric function TcLo (E_n), CPM0, and Gaussian. The red solid lines represent the Bose-Einstein model approximation.

The amplitude parameters of the MDF contributions are found to be almost constant for all temperatures. Solely the Pol contribution slightly enlarges with increasing temperature, which is reflected in the slight increase of the refractive index. Thus, we conclude that the density of states is affected by the temperature only for higher bands. The broadening parameters Γ of the MDF contributions increase with temperature as expected due to enhanced electron-phonon scattering. Caused in the large scatter of our data, the individual contributions of the interaction with acoustic and optical phonons cannot be separated, but a simplified linear approximation yields:

$$\Gamma_{\text{TcLo}}(T) = 400 (\pm 3) \text{ meV} + 0.26 (\pm 0.02) \text{ meV/K T},$$

$$\Gamma_{\text{CPM0}}(T) = 28 (\pm 2) \text{ meV} + 0.03 (\pm 0.01) \text{ meV/K T}.$$

For $\Gamma_{\text{TcLo}}(T)$, hints for a weaker increase at low temperatures are found in the data, thus applying the Bose-Einstein model as a simplest non-linear approximation the following parameters are found:

$$\Gamma_{\text{TcLo}}(0 \text{ K}) = 406 (\pm 3) \text{ meV},$$

$$E_{\text{BE-TcLo-}\Gamma} = 16 (\pm 7) \text{ meV},$$

$$\alpha_{\text{BE-TcLo-}\Gamma} = -0.34 (\pm 0.05) \text{ meV/K}.$$

The energy redshift of the indirect absorption edge between cryogenic and room temperatures was found in Ref. 13 for single crystals to be ≈ 200 meV, which is twice that observed here for the energy parameters of the TcLo oscillator. At low temperature, the absorption edge at energy $E_{\text{ind}} + E_{\text{ph}}$ (E_{ind} : energy of the intrinsic indirect band gap, E_{ph} : phonon energy) caused by phonon emission dominantly determines the lineshape of the DF; while at high temperature phonon absorption starting at $E_{\text{ind}} - E_{\text{ph}}$ strongly contributes. The TcLo function used here does not allow to directly distinguish between those contributions. The contribution of phonon absorption mainly affects the weak low energy absorption tail. Considering that in the TcLo model the low energy tail of the Lorentzian contribution superimposed by the quadratic Tauc absorption mimics the phonon

emission absorption edge, the upcoming phonon absorption is reflected in their broadening parameter. Thus, the increase in broadening $\Delta\Gamma_{\text{TcLo}} \approx 80 \text{ meV}$ is related to the increasing phonon absorption and $E_{\text{ph}} = 1/2 \Delta\Gamma_{\text{TcLo}} \approx 40 \text{ meV}$. It follows that the temperature dependence of the TcLo energy parameters has to be the same as that of the intrinsic band gap. The differences in the electron-phonon coupling strengths and effective phonon energies between the thin film and bulk crystals may be related to different crystal qualities.¹⁸ The weaker band gap shrinkage is beneficial for applications in transparent electronics.

As mentioned above, $E_{\text{CPM0}}(T)$ shows an even smaller slope reflected by its α_{BE} which is half of that of the TcLo energies. This surprising effect may be understood in terms of contributions of different electronic orbitals to the topmost valence bands. It is predicted theoretically^{3,4,8} that the contribution to the density of states closest to the valence band edge are dominantly of *s*- and *p*-type while the contribution of *d*-orbitals peaks some tens to hundred meV below. Those states should be less strongly affected by lattice vibrations because they interact less strongly with those of neighbouring atoms. This indicates that the CPM0 contribution should be caused by transitions involving In *d*-orbitals.

In conclusion, we have determined the DF of a bcc-In₂O₃ thin film in the wide spectral range of 0.5–8.5 eV and for temperatures 10–300 K. We have derived the refractive index dispersion, the absorption coefficient, and energy parameters of electronic transitions. From their temperature evolution, we have derived electron-phonon interaction properties. We found for the thin film weaker electron-phonon interaction compared to bulk single crystals causing also a weaker band gap shrinkage with increasing temperature which is beneficial for transparent electronic applications. Further we discussed excitonic effects possibly contributing to the dielectric function by applying two different parameterized models.

We acknowledge S. Müller for AFM measurements, G. Ramm for the PLD target preparation, H. Hochmuth for the film growth, as well as H. Franke and C. Sturm for comments on the manuscript and valuable discussions. This work was supported within the framework of EFRE (SAB

100132251). M.B. and C.K. were funded by the European Union and the Free State of Saxony.

- ¹R. Gupta, K. Ghosh, S. Mishra, and P. Kahol, *Thin Solid Films* **516**, 3204 (2008).
- ²H. von Wenckstern, D. Splith, F. Schmidt, M. Grundmann, O. Bierwagen, and J. S. Speck, *Appl. Phys. Lett. Mater.* **2**, 046104 (2014).
- ³S. Zh. Karazhanov, P. Ravindran, P. Vajeeston, A. Ulyashin, T. G. Finstad, and H. Fjellvåg, *Phys. Rev. B* **76**, 075129 (2007).
- ⁴F. Fuchs and F. Bechstedt, *Phys. Rev. B* **77**, 155107 (2008).
- ⁵P. Erhart, A. Klein, R. G. Egdell, and K. Albe, *Phys. Rev. B* **75**, 153205 (2007).
- ⁶A. Walsh, J. L. F. Da Silva, S.-H. Wei, C. Körber, A. Klein, L. F. J. Piper, A. DeMasi, K. E. Smith, G. Panaccione, P. Torelli, D. J. Payne, A. Bourlange, and R. G. Egdell, *Phys. Rev. Lett.* **100**, 167402 (2008).
- ⁷M. Ramzan, Y. Li, and R. Ahuja, *Solid State Commun.* **172**, 37 (2013).
- ⁸P. D. C. King, T. D. Veal, F. Fuchs, Ch. Y. Wang, D. J. Payne, A. Bourlange, H. Zhang, G. R. Bell, V. Cimalla, O. Ambacher, R. G. Egdell, F. Bechstedt, and C. F. McConville, *Phys. Rev. B* **79**, 205211 (2009).
- ⁹R. L. Weiher and R. P. Ley, *J. Appl. Phys.* **37**, 299 (1966).
- ¹⁰T. Hamberg, C. G. Granqvist, K. F. Berggren, B. E. Sernelius, and L. Engström, *Phys. Rev. B* **30**, 3240 (1984).
- ¹¹M. Girtana and G. Folcher, *Surf. Coat. Technol.* **172**, 242 (2003).
- ¹²L. Miao, S. Tanemura, Y. G. Cao, and G. Xu, *J. Mater. Sci.: Mater. Electron.* **20**, S71 (2009).
- ¹³K. Irschscher, M. Naumann, M. Pietsch, Z. Galazka, R. Uecker, T. Schulz, R. Schewski, M. Albrecht, and R. Fornari, *Phys. Status Solidi A* **211**, 54 (2014).
- ¹⁴C. Kranert, R. Schmidt-Grund, and M. Grundmann, *Phys. Status Solidi RRL* **8**, 554 (2014).
- ¹⁵See supplementary material at <http://dx.doi.org/10.1063/1.4896321> for more information on structural properties as well as details of the spectroscopic ellipsometry model analysis and the used model functions.
- ¹⁶H. Fujiwara, *Spectroscopic Ellipsometry: Principles and Applications* (John Wiley and Sons, 2007).
- ¹⁷R. Schmidt-Grund, C. Kranert, T. Böntgen, H. v. Wenckstern, H. Krauß, and M. Grundmann, *J. Appl. Phys.* **116**, 053510 (2014).
- ¹⁸R. Schmidt-Grund, T. Lühmann, T. Böntgen, H. Franke, D. Opper, M. Lorenz, and M. Grundmann, *J. Appl. Phys.* **114**, 223509 (2013).
- ¹⁹D. Beena, R. Vinodkumar, I. Navas, G. Rajan, and V. P. Mahadevan Pillai, *Mater. Sci. Eng., B* **174**, 59 (2010).
- ²⁰Z. P. Wei, D. L. Guo, B. Liu, R. Chen, L. M. Wong, W. F. Yang, S. J. Wang, H. D. Sun, and T. Wu, *Appl. Phys. Lett.* **96**, 031902 (2010).
- ²¹C.-H. Ho, C.-H. Chan, L.-C. Tien, and Y.-S. Huang, *J. Phys. Chem. C* **115**, 25088 (2011).
- ²²G. E. Jellison and F. A. Modine, *Appl. Phys. Lett.* **69**, 371 (1996); **69**, 2137 (1996).
- ²³C. Tanguy, *Phys. Rev. Lett.* **75**, 4090 (1995); **76**, 716 (1996).
- ²⁴C. Tanguy, *Phys. Rev. B* **60**, 10660 (1999).
- ²⁵S. Adachi, *Phys. Rev. B* **35**, 7454 (1987).
- ²⁶H. Yoshikawa and S. Adachi, *Jpn. J. Appl. Phys., Part 1* **36**, 6237 (1997).
- ²⁷L. Viña, S. Logothetidis, and M. Cardona, *Phys. Rev. B* **30**, 1979 (1984).